Temperature distribution of edge diode-pumped laser slab

M. H. MOGHTADER DINDARLU[*,a], M. KAVOSH TEHRANI[b], GH. SOLOOKINEJAD[c], A. MALEKI[b], M. JABBARI[d], M. NAFAR[d], R. TOFIGH MOVALU[b]

[a]*Young Researchers and Elite Club, Marvdasht branch, Islamic Azad University, Marvdasht, Iran*
[b]*Institute of Optics and Laser, Malek-ashtar University of Technology, Shahin Shahr, Postal Code: 83145/115, Iran*
[c]*Department of Physics, Marvdasht branch, Islamic Azad University, Marvdasht, Iran*
[d]*Department of Electronic Engineering, Marvdasht branch, Islamic Azad University, Marvdasht, Iran*

Since determination of temperature distribution inside the laser gain medium is essential for the evaluation of induced thermo-optic effects on laser operation, in this paper, an analytical model is presented for temperature distribution of edge diode-pumped laser slab by Green's function method. To solve the heat equation, Robin boundary conditions is considered because four lateral faces of slab are cooled by water. For an example, the 2D and 3D temperature distributions are plotted and our analytical model is validated by numerical solution based on Finite Element Method (FEM). The results show that our model has very good agreement with numerical solution. Furthermore, dependence of the temperature distribution on absorbed pump power is shown.

(Received February 4, 2018; accepted August 9, 2018)

Keywords: Temperature distribution, Laser slab, Edge-pumping, Robin boundary conditions

1. Introduction

High-power high-efficiency Diode-Pumped Solid State Lasers (DPSSL) have been widely used in military and industrial applications. But these lasers (especially rod geometry lasers) are always limited by the onset of deleterious effects such as thermal lensing, stress birefringence or biaxial focusing. To overcome these limitations on rod-shaped lasers, a number of designs including axial-gradient lasers, slab-shaped gain media, disk, and active mirror lasers have been proposed. Among them, the rectangular-slab laser is of great interest because it provides large cooling surfaces, and significantly reduces thermal stress-induced birefringence [1-4]. The slab gain medium geometry with zigzag laser propagation has traditionally been used to scale solid-state lasers to high powers by averaging out the thermal gradient induced distortion over the optical path [5-8]. Slab lasers are basically of three main types: end-pumping, edge-pumping, and side-pumping. End-pumped slab is attractive for good overlap between the pump volume and the laser mode, but suffers from small pump area, which limits the capability in power scaling per volume of the slab [9, 10]. In side-pumping, because of the short absorption path (thickness of slab), the pump efficiency may be relatively low unless a highly doped slab is used. In an edge-pumped slab, the pump light is incident on the middle-sized faces and propagates in the general direction of the slab's width. Pumping along the slab width allows a longer absorption path and hence lower doping; moreover, there are better choices for cooling since the largest faces of slab are not pumped [11-15]. Therefore, the edge-pumped slab laser has engineering advantages in high power slab laser's applications.

Optimizing the laser operation in presence of thermal effects needs temperature distribution inside the gain medium. Therefore, determination of temperature distribution inside the laser gain medium is essential for the evaluation of induced thermo-optic effects on laser operation. Solving the heat differential equation and considering boundary conditions give the temperature distribution. To obtain the temperature distribution of laser crystal, there are many software such as ANSYS, COMSOL, Flex PDE and LASCAD all of which are based on finite element method (FEM). However, an analytical model can be a more straightforward method for this purpose. For laser rod, many analytical models of temperature distribution have been reported [1,16-21]. Analytical calculations of the thermal effects in slab geometry lasers have been made by Eggleston et al. [16] and Kane, Eggleston and Byer [22]. These authors were primarily concerned with applying their analyses to lamp-pumped slabs. The thermal effects of an Nd:YVO_4 slab laser was reported by Ma et al. [23]. Their model is based on simple boundary conditions in which the slab was assumed to be infinitely long along one of the axes of the Cartesian coordinate system. Shi et al. [24] also reported the solution of the heat equation for a cubic geometry. They, too, adopted a simple boundary condition in which the temperature of all six faces was taken to be zero and constant. Only recently, did Sabaeian et al. [25] introduce an analytical solution of the heat equation for a longitudinally pumped cubic solid-state laser (End-pumping).

In this paper, for the first time to the best of our knowledge, a new analytical model of the temperature distribution is presented in edge diode-pumped laser slab with Robin boundary conditions by Green's function method. Pumping is done from the middle-sized faces of laser slab. Cooling is done by water sealing technology in which four lateral faces of slab are in contact with water. Two end-faces are in contact with the surrounding air. Therefore, we should consider Robin boundary conditions for the solution of the heat equation that is a precise and real boundary condition. Our analytical model is validated by numerical solution based on FEM. The results show that our model has very good agreement with numerical solution. This model can be used to extract other models for thermal effects such as thermal stress, stress birefringence and thermal lensing.

2. Heat equation

The three-dimensional heat conduction equation is written as

$$K\nabla^2 T(x,y,z)+Q(x,y,z)=0 \qquad (1)$$

where K is thermal conductivity and $Q(x,y,z)$ is the heat source defined as deposited power per unit volume. Fig. 1 shows that width, thickness, and length of laser slab are in x, y, and z directions, respectively ($0\le x\le a$, $0\le y\le b$, $0\le z\le c$). Also, it shows which slab is pumped from two-edges (planes $x=0, x=a$).

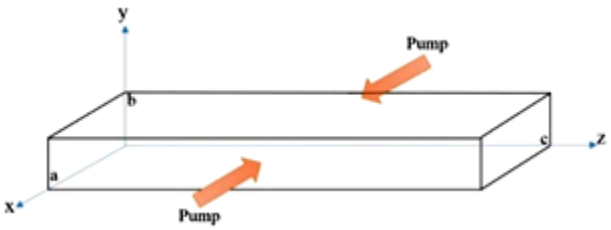

Fig. 1. The edge-pumped laser slab geometry in Cartesian coordinate

3. Pump configuration

The main challenge for the edge-pumped slab geometry is to achieve uniform pump absorption along the width since optical distortions of the crystal in this direction are not compensated by the zigzag path. For unsaturated absorption of the pump light, achieving perfectly uniform pump absorption is not possible. The slab edges near the pump source are always pumped harder than the slab center [26]. For edge-pumping configuration, Rutherford et al. showed that the absorbed pump power density as a function of the position x along the slab width is given as Hyperbolic function. The validity of this model was shown by comparison with experiment [27]. Consequently, the relevant heat source can be written as follows:

$$Q(x,y,z)=\frac{\eta P_{abs}\alpha}{bL\left[1-R_p\exp(-\alpha a)\right]}\exp\left(-\frac{\alpha a}{2}\right) .\cosh\left[\alpha\left(x-\frac{a}{2}\right)\right] \qquad (2)$$

where P_{abs} is absorbed power in the laser slab, η is the fraction of absorbed power converted to heat, α is pump absorption coefficient, R_p is the average pump reflectivity of the edge faces, L is the pump length and b is the thickness of laser slab.

4. Boundary conditions

We consider a cooling chamber for laser slab in which four faces ($x=0, x=a, y=0, y=b$) are in contact with water. In other words, these faces transfer heat by force convection. Therefore, for them, the following boundary conditions are assumed:

$$\frac{\partial T(x,y,z)}{\partial x}=\frac{h_w}{K}\left(T_w-T(x,y,z)\right),\quad x=0,a \qquad (3)$$

$$\frac{\partial T(x,y,z)}{\partial y}=\frac{h_w}{K}\left(T_w-T(x,y,z)\right),\quad y=0,b \qquad (4)$$

where h_w is force convection heat transfer coefficient with cooling-water and T_w is cooling water temperature. Two end-faces ($z=0, z=c$) are in contact with the surrounding air. In other words, these faces transfer heat by free convection. Their boundary conditions are written as:

$$\frac{\partial T(x,y,z)}{\partial z}=\frac{h_a}{K}\left(T_a-T(x,y,z)\right),\quad z=0,c \qquad (5)$$

where h_a is free convection heat transfer coefficient with air and T_a is room temperature. According to equations (3-5), Robin boundary conditions will exist for heat equation. Since these boundary conditions are real and precise, we solve heat equation and introduce a new analytical model for temperature distribution. Usually the laser slabs have the Brewster-angled input and output faces due to the convenient alignment, minimum optical loss and maintaining polarization. These slabs consist of a doped region diffusion bonded to un-doped end caps where the doped region is only pumped and cooled. It means that only this part is placed in the cooling cavity (in contact with water). Therefore, we can use the Green's function method for this region. Even if these end caps are also doped, again usually they are placed out of the cooling cavity. It means that we can use the Green's function method for pumped and cooled region.

5. Solution and results

According to equations (1-5), we can obtain the Green's function for our problem. The Green's function construction is stipulated by solving homogeneous equation (1), or the Laplace equation, by satisfying the boundary conditions and by its holding throughout the domain [28]. Consequently, the Green's function becomes:

$$G(x,y,z,\xi,\eta,\zeta) = \sum_{n=1}^{\infty}\sum_{m=1}^{\infty}\sum_{s=1}^{\infty}\frac{\varphi_n(x)\varphi_n(\xi)\psi_m(y)\psi_m(\eta)\chi_s(z)\chi_s(\zeta)}{\|\varphi_n\|^2\|\psi_m\|^2\|\chi_s\|^2\left(\mu_n^2+\lambda_m^2+\nu_s^2\right)} \quad (6)$$

where

$$\varphi_n(x) = \cos(\mu_n x) + \frac{h_w}{K\mu_n}\sin(\mu_n x) \quad (7)$$

$$\psi_m(y) = \cos(\lambda_m y) + \frac{h_w}{K\lambda_m}\sin(\lambda_m y) \quad (8)$$

$$\chi_s(z) = \cos(\nu_s z) + \frac{h_a}{K\nu_s}\sin(\nu_s z) \quad (9)$$

and

$$\|\varphi_n\|^2 = \frac{h_w}{K\mu_n^2} + \frac{a}{2}\left(1+\frac{h_w^2}{K^2\mu_n^2}\right) \quad (10)$$

$$\|\psi_m\|^2 = \frac{h_w}{K\lambda_m^2} + \frac{b}{2}\left(1+\frac{h_w^2}{K^2\lambda_m^2}\right) \quad (11)$$

$$\|\chi_s\|^2 = \frac{h_a}{K\nu_s^2} + \frac{c}{2}\left(1+\frac{h_a^2}{K^2\nu_s^2}\right) \quad (12)$$

where $\mu_n, \lambda_m, \upsilon_s$ are positive roots of the following transcendental equations:

$$\frac{\tan(\mu a)}{\mu} = \frac{2Kh_w}{\mu^2K^2 - {h_w}^2} \quad (13)$$

$$\frac{\tan(\lambda b)}{\lambda} = \frac{2Kh_w}{\lambda^2K^2 - {h_w}^2} \quad (14)$$

$$\frac{\tan(\nu c)}{\nu} = \frac{2Kh_a}{\nu^2K^2 - {h_a}^2} \quad (15)$$

By using Green's function (6), we solved the heat equation; and consequently, the following expression was obtained for temperature distribution (The details of the calculations have been presented in Appendix A).

$$T(x,y,z) = \sum_{n=1}^{\infty}\sum_{m=1}^{\infty}\sum_{s=1}^{\infty}\left\{\frac{\varphi_n(x)\psi_m(y)\chi_s(z)}{\|\varphi_n\|^2\|\psi_m\|^2\|\chi_s\|^2\left(\mu_n^2+\lambda_m^2+\nu_s^2\right)} \times\left[\begin{array}{l} ABCD + q_1CB\left(1+\varphi_n(a)\right) \\ +q_1EB\left(1+\psi_m(b)\right)+q_2CE\left(1+\chi_s(c)\right)\end{array}\right]\right\} \quad (16)$$

where

$$A = \frac{\eta P_{abs}\alpha\exp\left(-\frac{\alpha a}{2}\right)}{KbL\left[1-R_p\exp(-\alpha a)\right]} \quad (17)$$

$$B = \frac{2\sin\left(\frac{\nu_s c}{2}\right)\chi_s\left(\frac{c}{2}\right)}{\nu_s} \quad (18)$$

$$C = \frac{2\sin\left(\frac{\lambda_m b}{2}\right)\psi_m\left(\frac{b}{2}\right)}{\lambda_m} \quad (19)$$

$$D = \frac{1}{\mu_n\left(\alpha^2+\mu_n^2\right)}\times\left\{\begin{array}{l}\sin(a\mu_n)\left[\frac{\alpha h_w}{K}\sinh\left(\frac{\alpha a}{2}\right)+\mu_n^2\cosh\left(\frac{\alpha a}{2}\right)\right] \\ +2\alpha\mu_n\sinh\left(\frac{\alpha a}{2}\right)\cos^2\left(\frac{a\mu_n}{2}\right) \\ +\frac{2\mu_n h_w}{K}\cosh\left(\frac{\alpha a}{2}\right)\sin^2\left(\frac{a\mu_n}{2}\right)\end{array}\right\} \quad (20)$$

$$E = \frac{2\sin\left(\frac{\mu_n a}{2}\right)\varphi_n\left(\frac{a}{2}\right)}{\mu_n} \quad (21)$$

$$q_1 = \frac{h_w T_w}{K},\ q_2 = \frac{h_a T_a}{K} \quad (22)$$

In equation (16), there is a summation on m, n, and s parameters that upper bound is infinity. The indexes of summation indicate the positive roots number of transcendental equations (13-15). In process of extracting result, an initial value is chosen for the upper bound of summation (for example 50) then by increasing it, the result is converged to the accurate and final result. In the next section, to get the results and graphs, we have choose 700 for the upper bound of summation. Therefore, it can be said that a meaningful limit for summation is 700.

6. Comparison with numerical solution

In this section, our analytical model is tested as an example and it is compared with the numerical results obtained by FEM. In this example, we consider dual edge-pumped Nd:YAG laser slab with dimensions $12\times6\times100$ mm. In this configuration, the slab is pumped from the middle-sized faces ($x=0,12$ mm) as shown in Fig. 1. It is assumed that four lateral faces of slab are placed in water-cooling cavity in which water (with temperature of 298 K) flows at a specific rate on these faces. Two end-faces of slab are in contact with the surrounding air. All parameter values are listed in Table 1. Our analytical model can be applied for all of laser slab's geometry (With any thickness and cross-section dimensions such as cube-shape crystal) if the absorbed pump profile equal to equation (2) for edge-pumping configuration.

Table 1. Numerical values of parameters

Parameters	Parameter name	Values (units)
a	Width of slab	12 mm
b	Thickness of slab	6 mm
c	Length of slab	100 mm
η	Fraction of absorbed power converted to heat	0.3
P_{abs}	Absorbed pump power	600 W
α	Absorption coefficient	0.35 mm^{-1}
ω_p	Width of the Gaussian distribution in x and y-direction	3 mm
L	Length of pumping	100 mm
K	Thermal conductivity	10.5 $Wm^{-1}K^{-1}$
h_a	Free-convection heat transfer coefficient with air	50 $WK^{-1}m^{-2}$
h_w	Force convection heat transfer coefficient with cooling-water	20000 $WK^{-1}m^{-2}$
T_a	Room temperature	298 K
T_w	Cooling-water temperature	298 K

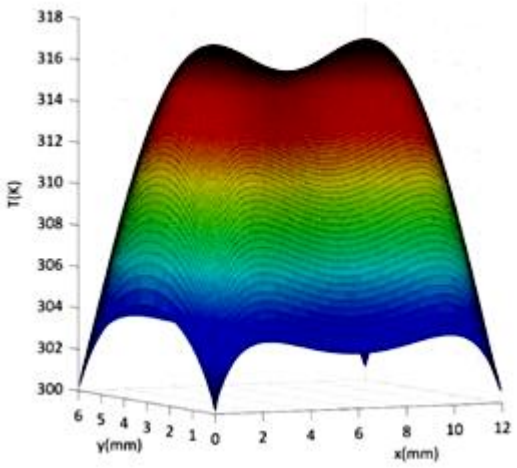

Fig. 2. 3D temperature distribution in x-y plane at z = 50mm for edge-pumped slab

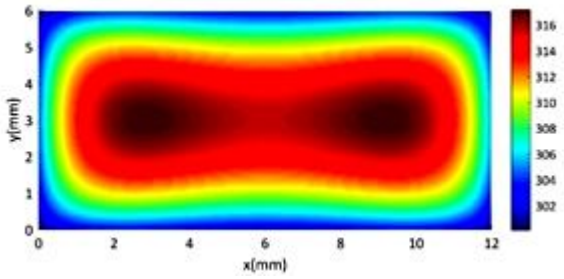

Fig. 3. 2D temperature profile in x-y plane at z = 50mm for edge-pumped slab

To investigate the temperature distribution in the thickness direction of the slab, we drew the temperature distribution along the y-axis (at $z=50$ mm, $x=6$ mm) as shown in Fig. 4. In this figure, the solid curve shows the results of our analytical model and the dotted curve shows the numerical results. It is clear from the figure, that there is very good agreement between our analytical model and the numerical solution. According to Fig. 4, the temperature asymmetry in the direction of the slab thickness is clearly shown.

According to equation (16) and Table 1, the three-dimensional temperature distribution in x-y plane at $z=50$ mm has been plotted in Fig. 2. The two-dimensional temperature profile of Fig. 2, has been presented in Fig. 3. It is apparent from Fig. 3 that temperature distribution of laser slab is symmetric in x-direction (width of slab) and y-direction (thickness of slab).

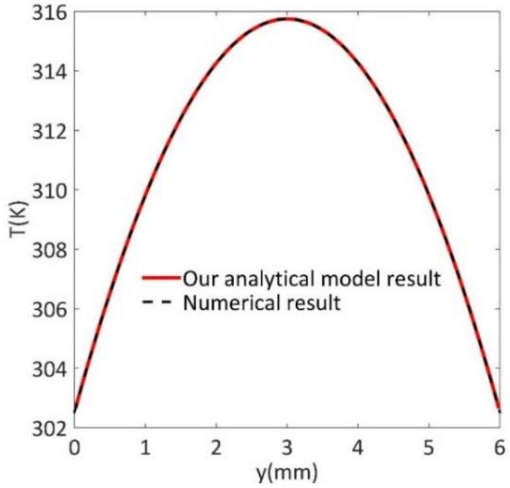

Fig. 4. Temperature distribution along the y-axis (slab thickness) at z = 50mm, x = 6mm for edge-pumped slab

We then drew the temperature distribution along the x-axis (at $z = 50\,\text{mm},\ y = 3\text{mm}$) as shown in Fig. 5 (maximum temperature of laser slab is 317.2 K). In this figure, also good agreement is seen between our analytical model and the numerical solution. Fig. 5, clearly shows that the temperature distribution is symmetric in the width direction of the slab for dual edge-pumping configuration. According to this figure, the temperature of pump faces ($x = 0,12\,\text{mm}$) is about 304.9K.

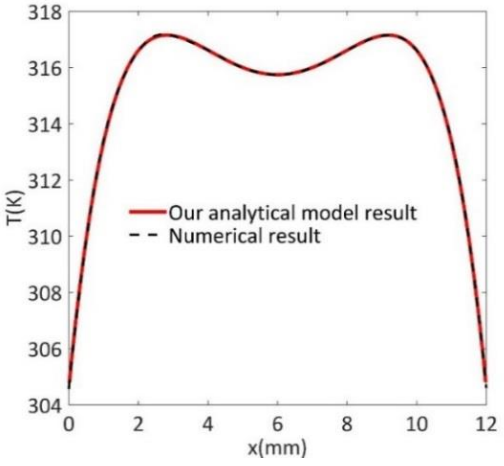

Fig. 5. Temperature distribution along the x-axis (slab width) at z = 50mm, y = 3mm for edge-pumped slab

Finally, the temperature distribution along the z-axis (at $x = 6\,\text{mm}, y = 3\text{mm}$) has been drawn in Fig. 6, for edge-pumping. In this figure, the constant temperature along the slab length can be seen. Results of our analytical model and the numerical solution are also close together.

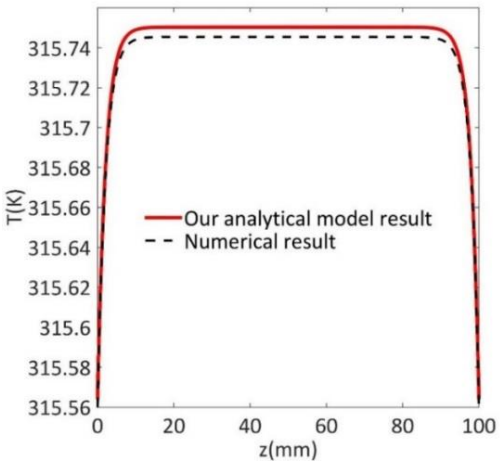

Fig. 6. Temperature distribution along the z-axis (slab length) at x = 6 mm, y = 3 mm for edge-pumped slab

7. Dependence of temperature distribution on absorbed pump power

To show the dependence of the temperature distribution on absorbed pump power, we plot the curve of temperature (along of x-axis) for various absorbed pump power. According to the example presented in previous section, the parameters of Table 1, four absorbed pump power ($P_{abs} = 500, 600, 700, 800\text{W}$), and equation (16), the temperature distributions along x-axis for edge-pumping configuration is shown in Fig. 7. This figure shows how the temperature of laser slab rises by increasing the absorbed pump power.

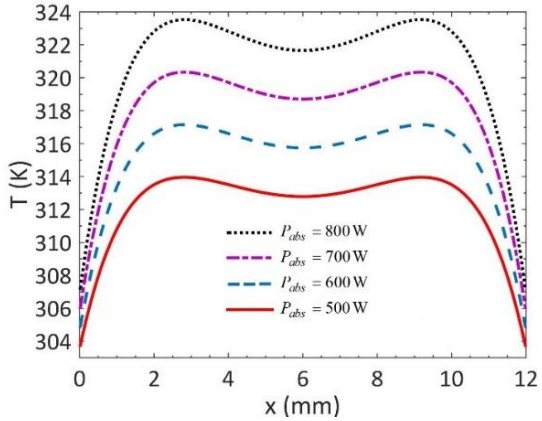

Fig. 7. Temperature distribution along the x-axis (slab width) at z = 50mm, y = 3mm for various absorbed pump power

8. Conclusions

Since, to the best of our knowledge, there is no precise and comprehensive analytical model of temperature distribution for edge pumped laser slabs with Robin boundary conditions, we derived an analytical model for

temperature distribution of laser slab. Our analytical model was tested for an example (edge diode-pumped Nd:YAG lase slab). By drawing many temperature curves, there was very good agreement between our analytical model and the numerical solution. This model can be used to extract the other models for thermal effects such as thermal stress, stress birefringence and thermal lensing. For future investigation, this method can be considered for temperature distribution of anisotropic laser slabs such that Nd:YVO_4 and Nd:$GdYVO_4$. Also, it can be extended for face-pumping configuration of laser slabs.

Appendix A

Heat equation (1) can be rewritten as follows:

$$\nabla^2 T(x,y,z) + \frac{Q(x,y,z)}{K} = 0 \tag{A.1}$$

According to the obtained Green's function (6) for heat equation (A.1) and Robin boundary conditions (3-5), the following solution can be written [28]:

$$\begin{aligned} T(x,y,z) = {} & \int_0^a\int_0^b\int_0^c \frac{Q(x,y,z)}{K} G(x,y,z,\xi,\eta,\zeta)\,d\zeta\,d\eta\,d\xi \\ & + \int_0^b\int_0^c \frac{h_w T_w}{K} G(x,y,z,0,\eta,\zeta)\,d\zeta\,d\eta \\ & + \int_0^b\int_0^c \frac{h_w T_w}{K} G(x,y,z,a,\eta,\zeta)\,d\zeta\,d\eta \\ & + \int_0^a\int_0^c \frac{h_w T_w}{K} G(x,y,z,\xi,0,\zeta)\,d\zeta\,d\xi \\ & + \int_0^a\int_0^c \frac{h_w T_w}{K} G(x,y,z,\xi,b,\zeta)\,d\zeta\,d\xi \\ & + \int_0^a\int_0^b \frac{h_a T_a}{K} G(x,y,z,\xi,\eta,0)\,d\eta\,d\xi \\ & + \int_0^a\int_0^b \frac{h_a T_a}{K} G(x,y,z,\xi,\eta,c)\,d\eta\,d\xi \end{aligned} \tag{A.2}$$

In equation (A.2), the triple integral (first integral) is responsible for temperature difference caused by the heat deposited in the laser slab, and six double integrals satisfy the boundary condition on four lateral faces of laser slabs. First, the triple integral is solved. By substituting equations (2) and (6) in the triple integral, it can be written as follows:

$$\begin{aligned} & \int_0^a\int_0^b\int_0^c \frac{Q(x,y,z)}{K} G(x,y,z,\xi,\eta,\zeta)\,d\zeta\,d\eta\,d\xi = \\ & = \frac{\eta P_{abs}\alpha \exp\left(-\frac{\alpha a}{2}\right)}{KbL\left[1 - R_p \exp(-\alpha a)\right]} \times \\ & \sum_{n=1}^{\infty}\sum_{m=1}^{\infty}\sum_{s=1}^{\infty} \frac{\varphi_n(x)\psi_m(y)\chi_s(z)}{\|\varphi_n\|^2 \|\psi_m\|^2 \|\chi_s\|^2 \left(\mu_n^2 + \lambda_m^2 + \nu_s^2\right)} \\ & \times \left\{ \int_0^a \varphi_n(\xi)\cosh\left[\alpha\left(\xi - \frac{a}{2}\right)\right] d\xi \times \int_0^b \psi_m(\eta)\,d\eta \times \int_0^c \chi_s(\zeta)\,d\zeta \right\} \end{aligned} \tag{A.3}$$

Now, the solutions of three integrals are found in braces.

$$B = \int_0^c \chi_s(\zeta)\,d\zeta \tag{A.4}$$

By substituting equation (9) in (A.4), after simplification, we can write:

$$B = \frac{2\sin\left(\frac{\nu_s c}{2}\right)\chi_s\left(\frac{c}{2}\right)}{\nu_s} \tag{A.5}$$

where $\chi_s\left(\frac{c}{2}\right) = \cos\left(\frac{\nu_s c}{2}\right) + \frac{h_a}{K\nu_s}\sin\left(\frac{\nu_s c}{2}\right)$ according to the equation (9).

The second integral is

$$C = \int_0^b \psi_m(\eta)\,d\eta \tag{A.6}$$

By substituting equation (8) in (A.6) and after simplification, it becomes:

$$C = \frac{2\sin\left(\frac{\lambda_m b}{2}\right)\psi_m\left(\frac{b}{2}\right)}{\lambda_m} \tag{A.7}$$

The third integral is

$$D = \int_0^a \varphi_n(\xi)\cosh\left[\alpha\left(\xi - \frac{a}{2}\right)\right] d\xi \tag{A.8}$$

By substituting equation (7) in (A.8), after calculating and simplification, we can write:

$$D=\frac{1}{\mu_n\left(\alpha^2+\mu_n^2\right)}\times\left\{\begin{array}{l}\sin(a\mu_n)\left[\dfrac{\alpha h_w}{K}\sinh\left(\dfrac{\alpha a}{2}\right)+\mu_n^2\cosh\left(\dfrac{\alpha a}{2}\right)\right]\\+2\alpha\mu_n\sinh\left(\dfrac{\alpha a}{2}\right)\cos^2\left(\dfrac{a\mu_n}{2}\right)\\+\dfrac{2\mu_n h_w}{K}\cosh\left(\dfrac{\alpha a}{2}\right)\sin^2\left(\dfrac{a\mu_n}{2}\right)\end{array}\right\} \tag{A.9}$$

Now, the triple integral (A.3) can be rewritten as follows:

$$\int_0^a\int_0^b\int_0^c\frac{Q(x,y,z)}{K}G(x,y,z,\xi,\eta,\zeta)d\zeta d\eta d\xi=$$
$$A\sum_{n=1}^{\infty}\sum_{m=1}^{\infty}\sum_{s=1}^{\infty}\frac{\varphi_n(x)\psi_m(y)\chi_s(z)}{\|\varphi_n\|^2\|\psi_m\|^2\|\chi_s\|^2\left(\mu_n^2+\lambda_m^2+\nu_s^2\right)}\{B\times C\times D\} \tag{A.10}$$

where $A=\dfrac{\eta P_{abs}\alpha\exp\left(-\dfrac{\alpha a}{2}\right)}{KbL\left[1-R_p\exp(-\alpha a)\right]}$

Now, six double integrals in equation (A.2) should be solved. Here, the first and second integrals are written as:

$$\int_0^b\int_0^c\frac{h_wT_w}{K}G(x,y,z,0,\eta,\zeta)d\zeta d\eta+\int_0^b\int_0^c\frac{h_wT_w}{K}G(x,y,z,a,\eta,\zeta)d\zeta d\eta \tag{A.11}$$

According to equation (6), we have:

$$G(x,y,z,0,\eta,\zeta)=$$
$$\sum_{n=1}^{\infty}\sum_{m=1}^{\infty}\sum_{s=1}^{\infty}\frac{\varphi_n(x)\varphi_n(0)\psi_m(y)\psi_m(\eta)\chi_s(z)\chi_s(\zeta)}{\|\varphi_n\|^2\|\psi_m\|^2\|\chi_s\|^2\left(\mu_n^2+\lambda_m^2+\nu_s^2\right)} \tag{A.12}$$

$$G(x,y,z,a,\eta,\zeta)=$$
$$\sum_{n=1}^{\infty}\sum_{m=1}^{\infty}\sum_{s=1}^{\infty}\frac{\varphi_n(x)\varphi_n(a)\psi_m(y)\psi_m(\eta)\chi_s(z)\chi_s(\zeta)}{\|\varphi_n\|^2\|\psi_m\|^2\|\chi_s\|^2\left(\mu_n^2+\lambda_m^2+\nu_s^2\right)} \tag{A.13}$$

Since $\varphi_n(0)=1$, by substituting equations (A.12) and (A.13) in (A.11), equation (A.11) can be rewritten as follows:

$$\sum_{n=1}^{\infty}\sum_{m=1}^{\infty}\sum_{s=1}^{\infty}\left\{\begin{array}{l}\dfrac{\varphi_n(x)\psi_m(y)\chi_s(z)}{\|\varphi_n\|^2\|\psi_m\|^2\|\chi_s\|^2\left(\mu_n^2+\lambda_m^2+\nu_s^2\right)}\\\times\dfrac{h_wT_w}{K}\left[1+\varphi_n(a)\right]\times\left(\displaystyle\int_0^b\psi_m(\eta)d\eta\times\int_0^c\chi_s(\zeta)d\zeta\right)\end{array}\right\} \tag{A.14}$$

In equation (A.14), the first and second integrals are equal to C and B, respectively. Therefore equation (A.11) becomes:

$$\sum_{n=1}^{\infty}\sum_{m=1}^{\infty}\sum_{s=1}^{\infty}\left\{\begin{array}{l}\dfrac{\varphi_n(x)\psi_m(y)\chi_s(z)}{\|\varphi_n\|^2\|\psi_m\|^2\|\chi_s\|^2\left(\mu_n^2+\lambda_m^2+\nu_s^2\right)}\\\times q_1CB\left[1+\varphi_n(a)\right]\end{array}\right\} \tag{A.15}$$

where $q_1=\dfrac{h_wT_w}{K}$.

Similarly, the third and fourth double integrals will become:

$$\sum_{n=1}^{\infty}\sum_{m=1}^{\infty}\sum_{s=1}^{\infty}\left\{\begin{array}{l}\dfrac{\varphi_n(x)\psi_m(y)\chi_s(z)}{\|\varphi_n\|^2\|\psi_m\|^2\|\chi_s\|^2\left(\mu_n^2+\lambda_m^2+\nu_s^2\right)}\\\times q_1BE\left[1+\psi_m(b)\right]\end{array}\right\} \tag{A.16}$$

where

$$E=\int_0^a\varphi_n(\xi)d\xi=\frac{2\sin\left(\dfrac{\mu_n a}{2}\right)\varphi_n\left(\dfrac{a}{2}\right)}{\mu_n} \tag{A.17}$$

Also, the fifth and sixth double integrals will become:

$$\sum_{n=1}^{\infty}\sum_{m=1}^{\infty}\sum_{s=1}^{\infty}\frac{\varphi_n(x)\psi_m(y)\chi_s(z)}{\|\varphi_n\|^2\|\psi_m\|^2\|\chi_s\|^2\left(\mu_n^2+\lambda_m^2+\nu_s^2\right)}\times q_2CE\left[1+\chi_s(c)\right] \tag{A.18}$$

where $q_2=\dfrac{h_aT_a}{K}$.

Consequently, according to equations (A.2), (A.10), (A.15), (A.16), and (A.18), the expression of temperature distribution can be derived as follows:

$$T(x,y,z)=\sum_{n=1}^{\infty}\sum_{m=1}^{\infty}\sum_{s=1}^{\infty}\left\{\begin{array}{l}\dfrac{\varphi_n(x)\psi_m(y)\chi_s(z)}{\|\varphi_n\|^2\|\psi_m\|^2\|\chi_s\|^2\left(\mu_n^2+\lambda_m^2+\nu_s^2\right)}\\\times\left[\begin{array}{l}ABCD+q_1CB\left(1+\varphi_n(a)\right)\\+q_1EB\left(1+\psi_m(b)\right)\\+q_2CE\left(1+\chi_s(c)\right)\end{array}\right]\end{array}\right\} \tag{A.19}$$

References

[1] W. Koechner, "Solid-state Laser Engineering", Springer, Berlin, (2006).

[2] Y. Chen, B. Chen, M. K. R. Patel, M. Bass, IEEE J. Quantum Electron. **40**, 909 (2004).

[3] Y. Chen, B. Chen, M. K. R. Patel, A. Kar, M. Bass,

IEEE J. Quantum Electron. **40**, 917 (2004).
[4] Y. Chen, B. Chen, M. Bass, Appl. Phys. B **8**, 75 (2005).
[5] G. F. Albrecht, J. M. Eggleston, J. J. Ewing, IEEE J. Quantum Electron. **22**, 2099 (1986).
[6] R. J. Shine, A. J. Alfrey, R. L. Byer, Opt. Lett. **20**, 459 (1995).
[7] R. J. St. Pierre, G. W. Holleman, M. Valley, H. Injeyan, J. G. Berg, R. C. Hilyard, M. Mitchell, M. E. Weber, J. Zamel, T. Engler, D. Hall, R. Tinti, J. Machan, IEEE J. Sel. Topics Quantum Electron. **3**, 64 (1997).
[8] R. J. St. Pierre, D. W. Mordaunt, H. Injeyan, J. G. Berg, R. C. Hilyard, M. E. Weber, M. G. Wickham, G. Harpole, Proc. SPIE **3264**, 2 (1998).
[9] G. D. Goodno, H. Komine, S. J. McNaught, S. B. Weiss, S. Redmond, W. Long, R. Simpson, E. C. Cheung, D. Howland, P. Epp, M. Webber, M. McClellan, J. Sollee, H. Injeyan, Opt. Lett. **31**, 1247 (2006).
[10] Y. F. Chen, T. M. Huang, C. F. Kao, C. L. Wang, S. C. Wang, IEEE J. Quantum Electron. **3**, 29 (1997).
[11] T. S. Rutherford, W. M. Tulloch, S. Sinha, R. L. Byer, Opt. Lett. **26**, 986 (2001).
[12] W. M. Tulloch, T. S. Rutherford, E. K. Gustafson, R. L. Byer, Proc. SPIE **3613**, 2 (1999).
[13] B. Chen, Y. Chen, J. Simmons, T. Y. Chung, M. Bass, Appl. Phys. B **82**, 413 (2006).
[14] T. Y. Fan, J. Quantum Electron. **29**, 1457 (1993).
[15] M. Bass, Photonics Spectra **39**, 110 (2005).
[16] J. M. Eggleston, T. J. Kane, K. Kuhn, J. Unternahrer, R. L. Byer, IEEE J. Quantum Electron. **QE-20**, 289 (1984).
[17] X. Wenjie, T. Siu-Chung, Y. L. Lam, L. Jingang, Y. Hongru, G. Jianhui, T. Wilson, Z. Feng, Opt. Laser Technol. **32**, 199 (2000).
[18] A. Montmerle Bonnefois, M. Gilbert, P. Y. Thro, J. M. Weulersse, Opt. Commun. **25**(9), 223 (2006).
[19] N. Hodgson, H. Weber, IEEE J. Quantum Electron. **QE-29**, 2497 (1993).
[20] U. O. Farrukh, P. Brockmann, Appl. Optics **32**, 2075 (1993).
[21] M. H. Moghtader Dindarlu, A. Maleki, H. Saghafifar, M. Kavosh Tehrani, S. Baghali, Laser Phys. **25**, 045001 (2015).
[22] T. J. Kane, J. M. Eggleston, R. L. Byer, IEEE J. Quantum. Electron. **21**, 1195 (1985).
[23] Z. Ma, D. Li, J. Gao, N. Wu, K. Du, Opt. Commun. **275**, 179 (2007).
[24] P. Shi, W. Chen, L. Li, A. Gan, Appl. Opt. **46**, 4046 (2007).
[25] M. Sabaeian, H. Nadgaran, L. Mousave, Appl. Opt. **47**, 2317 (2008).
[26] T. J. Kane, J. M. Eggleston, R. L. Byer, IEEE J. Quantum Electron. **QE-21**, 1195 (1985).
[27] T. S. Rutherford, W. M. Tulloch, E. K. Gustafson, R. L. Byer, IEEE J. Quantum. Electron. **36**, 205 (2000).
[28] A. D. Polianin, "Handbook of Linear Partial Differential Equations for Engineers and Scientists", Chapman & Hall/CRC (2002).

*Corresponding author: mh.moghtader@miau.ac.ir